Temperature Dependent Reflectance and Ellipsometry Studies on a $CsPbBr_3$ Single Crystal

Xiaoxuan Chen,[†] Yue Wang,[†,‡] Jizhong Song,[‡] Xiaoming Li,[‡] Jiayue Xu,[§] Haibo Zeng,[‡] and Handong Sun[*,†,∥,⊥]

[†]*Division of Physics and Applied Physics, School of Physical and Mathematical Sciences, Nanyang Technological University, Singapore 637371, Singapore*

[‡]*MIIT Key Laboratory of Advanced Display Materials and Devices, Institute of Optoelectronics and Nanomaterials, School of Materials Science and Engineering, Nanjing University of Science and Technology, Nanjing 210094, China*

[§]*Institute of Crystal Growth, School of Materials Science and Engineering, Shanghai Institute of Technology, Shanghai 201418, China*

[∥]*Centre for Disruptive Photonic Technologies (CDPT), Nanyang Technological University, Singapore 637371, Singapore*

[⊥]*MajuLab, CNRS-UCA-SU-NUS-NTU International Joint Research Unit, Singapore*

ABSTRACT

Inorganic halide perovskites have attracted enormous interest in recent years owing to their remarkable properties for next-generation optoelectronics. Yet their basic optical properties have been rarely explored, which failed to meet the demand of accelerating the progress of this emerging field. In this work, temperature dependent reflection spectroscopy and ellipsometry were carried out on a $CsPbBr_3$ bulk perovskite single crystal. Two discernable optical transitions at around 2.4 and 3.4 eV with opposite temperature dependence are observed, indicating the complexity of the carrier-phonon scattering process in perovskites. The intrinsic transition energy, exciton-phonon interaction, exciton polariton and strong oscillator strength ($\sim 1.3 \times 10^{30}$ rad^2/sec^2) of the three-dimensional Wannier-Mott excitons are revealed. We have acquired by ellipsometry measurement the wavelength dependent dielectric constants and the complex refractive indices which are vital for informed optical designs to achieve device performance optimization. Furthermore, the essential and elemental optical properties such as absorption coefficient, absorption cross-section, optical conductivity and dispersion relation of $CsPbBr_3$ are obtained. These parameters give insights in both fundamental physics and practical applications of $CsPbBr_3$ perovskites. This work unveils the photophysics of inorganic perovskites as well as offers approaches to identify the optical transitions and extract essential physical parameters, which can be utilized to explore other perovskite materials and nanostructures.

INTRODUCTION

Halide perovskite materials have been emerging as promising candidates for light harvesting and light emitting devices.[1] This kind of materials possesses high quantum yield, fast mobility of both electrons and holes, long diffusion length and facile bandgap tuning by mixing halides.[2] Compared to the organic-inorganic hybrid perovskites, all-inorganic lead halide perovskites have been reported to exhibit higher stabilities and competitive performances.[3-5] Nonetheless, all-inorganic perovskites were much less explored than organic-inorganic hybrid ones. It is urged to clarify the fundamental photophysics of the all-inorganic perovskites to explain their favorable properties and then make better use of them. We investigated in this work the basic properties of a $CsPbBr_3$ perovskite single crystal by ellipsometry and temperature dependent reflection spectroscopy. Ellipsometry and reflection spectroscopy are non-invasive and broad-spectral experiment tools to unveil the optical properties that are significant in fundamental understanding and practical applications. The spectral features identified by ellipsometry and reflectance imply the meaningful information of energy band structures of the material, which can be applied to compare with theoretical calculations and refine the vital electronic structure simulations. The wavelength dependent optical constants are prerequisites for robust optical models which provide guidelines to design and optimize optoelectronic devices, signifying both potentials and limitations.

Herein, bulk crystals were chosen to be characterized due to several reasons. First, bulk crystals retain the intrinsic properties of the material in contrast to thin films. The properties of the latter ones often depend on the methods of the synthesis, deposition, annealing and even the index of the solvent.[6-8] Moreover, the stretch and compression caused by the lattice mismatch between

the thin film and the substrate deforms the lattice and electronic structure of the material. Thus, sample to sample variations abound. Second, different from nanostructures such as quantum dots, nanorods and nanoplatelets, the intrinsic property of bulk perovskites will not be affected by quantum confinement effect which will influence the exciton behavior, absorption spectrum and carrier decay rate.[9] The properties of the intrinsic perovskite bulk crystals can then be rescaled to lower dimensional materials and be utilized as references for studies of vast morphologies of perovskites to infer the size and shape effects. Third, it was demonstrated that the photophysics of perovskites is closely linked to their grain sizes.[10] Single crystals with much less impurities, defects and grain boundaries, have shown superior performances over polycrystals and need to be further characterized for future applications.[11]

In this work, the fundamental photophysics of $CsPbBr_3$ perovskite bulk crystal is investigated. Two discernable transitions are observed in which the higher energy one is usually absent in photoluminescence spectrum. The different behaviors of the two transitions with respect to the temperature indicate the complexity of the electron-phonon scattering in perovskites. The dependence of the three-dimensional Wannier-Mott exciton peak positions and linewidths on temperature is analyzed by a Lorentzian model and the optical phonon energy is deduced. By measuring ellipsometry, the dielectric constants and complex refractive indices are extracted. Based on the optical constants acquired, dispersion relation, absorption coefficient, absorption cross-section and optical conductivity spectra are presented. Finally, the oscillator strength of $CsPbBr_3$ is estimated to be 1.3×10^{30} rad^2/sec^2. The large oscillator strength explains the excellent optical properties of perovskite and leads to a variety of possible applications in optoelectronic devices.

METHODS

Synthesis. The crystal was synthesized by modified Bridgman growth method with a four-zone furnace. The thorough fabrication process can be found in ref 12. The sample studied in this work was cut from the bulk crystal. The high degree of crystallinity was demonstrated by high resolution X-ray diffraction which showed very narrow linewidths in rocking curve measurement.[12]

Ellipsometry. Variable angle spectroscopic ellipsometry (VASE) is a non-destructive and highly sensitive instrument to study the fundamental optical properties of a material. It measures the change of polarization of light upon reflection. The perpendicular (s-) polarized light and the parallel (p-) polarized light behaves differently when reflected from the sample surface. The ratio of the reflection intensity of the s- and p- polarized light is portrayed by two parameters Ψ and Δ as $\tilde{r_p}/\tilde{r_s} = tan(\Psi)e^{i\Delta}$. See detail information in ref 13. The optical constants were extracted by CompleteEASE software (developed by J.A. Woollam Co.) utilizing B-spline polynomials,

$$B_i^0(x) = \begin{cases} 1, & t_i \le x \le t_{i+1} \\ 0 & \text{otherwise,} \end{cases} \tag{1a}$$

$$B_i^k(x) = \left(\frac{x - t_i}{t_{i+k} - t_i}\right) B_i^{k-1}(x) + \left(\frac{t_{i+k+1} - x}{t_{i+k+1} - t_{i+1}}\right) B_{i+1}^{k-1}(x), \tag{1b}$$

where k is the degree of polynomial splines, t_i is the connection point of polynomials and i is the knot index. B-spline model typically reduces the free parameters in fitting and the resulting correlations between parameters, and more significantly, it forces Kramers-Kronig consistency and ensures a physical plausible result can be obtained.

Temperature Dependent Reflection Spectroscopy. The reflection spectroscopy was conducted on the $CsPbBr_3$ perovskite bulk crystal from 10 K to room temperature in backscattering

configuration. Higher temperature measurements can be detrimental to the cryostat system, while these measurements would be beneficial for studies of solar cells under intense heat. The light source was provided by a halogen lamp, and the reflected light was collected and resolved by a monochromator and then recorded by a photomultiplier. The sample was kept in a helium-cooled cryostat with fused silica optical windows. A smooth-surface Quartz slip with no absorption peaks throughout the recorded spectrum is also measured as a reference. A chopper and a lock-in amplifier are employed to improve the signal-to-noise ratio. The reflection spectrum of unpolarized light at room temperature was also recorded by VASE in Fig. 2(e) as a reference to confirm the reliability of the temperature dependent reflection setup.

RESULTS AND DISCUSSION

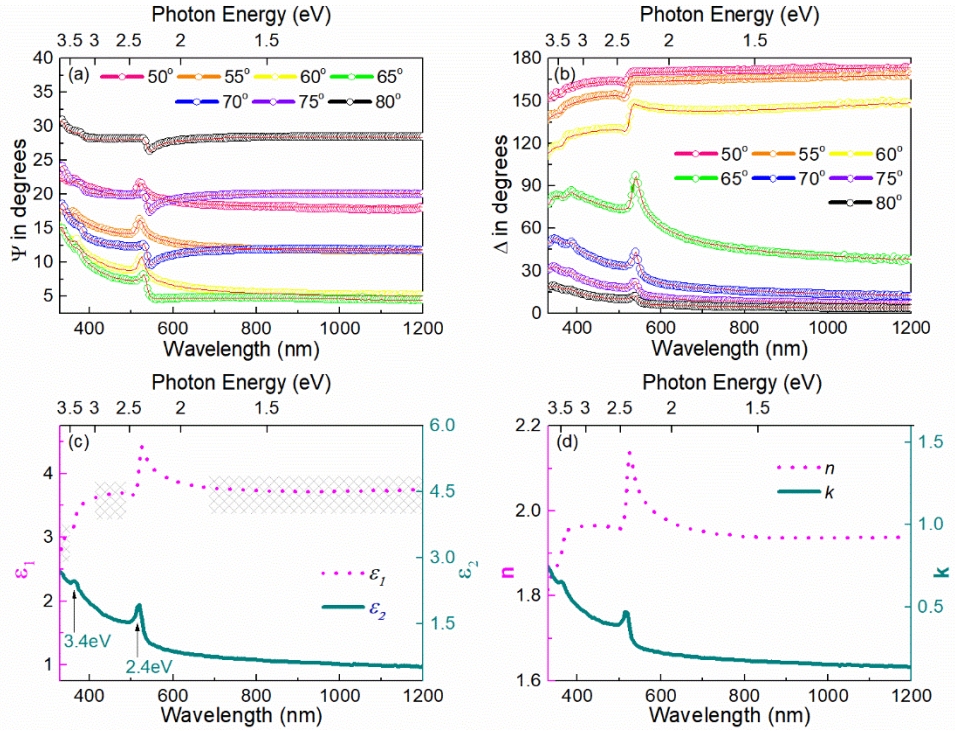

FIG. 1. (a) Ψ and (b) Δ measured by VASE on the $CsPbBr_3$ sample. The red lines show the fitting results of multi-angle analysis for both Ψ and Δ. (c) The dielectric constants ε_1(pink dash line) and ε_2 (blue solid line) and (d) the real part of the refractive index n (pink dash line) and extinction coefficient κ (blue solid line) extracted.

We first investigated the optical transitions and dielectric functions of $CsPbBr_3$ perovskites by VASE. Ψ and Δ from 50 degrees to 80 degrees are shown in Fig. 1(a) and 1(b). The measurements were taken at different positions on the sample and the consistency of the experiment data indicates the homogeneity of the sample. The mean square error (MSE) of the fitting result is 3.448, which confirms good agreement between the simulation and measurement. In Fig. 1(c). The imaginary part of the dielectric constant ε_2 reveals the optical transitions from valence band to conduction band, where an excitonic absorption peak at 2.4 eV can be clearly observed. In addition, a transition at higher energy in the UV region (ca. 3.4 eV) is also revealed, which was not observed in photoluminescence spectrum. Note that the real part ε_1 jumps to a

relatively constant value (highlighted by grey shades) after every optical transition with a general growing trend with decreasing of frequency (or increasing of wavelength). The reason is that every resonance from higher energy side will contribute to the dielectric constant at lower energy side according to

$$\varepsilon(\omega) = 1 + \sum_j \frac{f_j}{\omega_{0j}^2 - \omega^2 - i\omega\gamma_j}, \quad (2)$$

where ω_{0j} is the transition energy frequency, f_j is the oscillator strength and γ_j is the damping factor. This change of the dielectric constant around resonances is a typical phenomenon by Kramers-Kronig relationship. Thus, both real and imaginary part of the dielectric constant confirm the existence of two optical transitions. we will discuss more about these transitions in temperature dependent reflectance. After two optical transitions, the dielectric constant reaches a constant value of 3.73 that is close the result of 3.8 previously calculated by density functional theory (DFT).[14] In Fig. 1(d), the refractive index and the extinction coefficient over the spectrum range from near ultraviolet to near infrared are demonstrated. Both of them are important parameters for architecture design of optoelectronic devices.[15-17] The lower refractive index of perovskite material (compared with CIGS, GaAs and CdTe) for anti-reflection coating, together with the large extinction coefficient for light absorption and trapping, make perovskite ideal components in monolithic tandem solar cells to achieve higher efficiency beyond the conversion limit. [18-19]

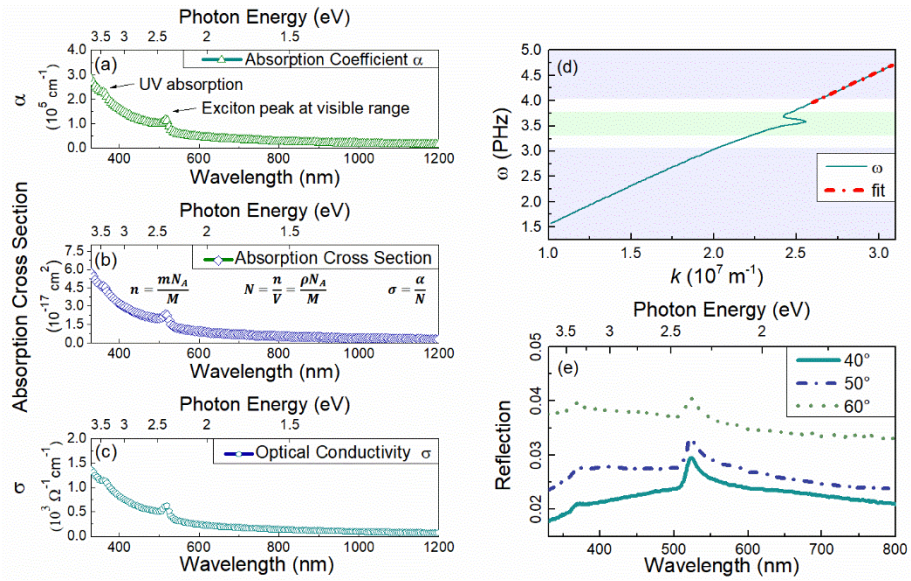

FIG. 2. (a) Absorption coefficient α, (b) absorption cross-section and (c) optical conductivity σ of $CsPbBr_3$ from near ultraviolet to near infrared. (d) Dispersion relation $\omega - k$ (blue solid line) with a linear fit (red dash line). (e) The reflection spectrum measured by VASE.

The absorption spectrum is acquired by $4\pi\kappa/\lambda$ (where λ is the wavelength) and shown in Fig. 2(a), the magnitude (~ 10^5 cm^{-1}) is consistent with other perovskites.[20] The peak at around 2.4 eV is the exciton absorption peak and that around 3.4 eV is the higher energy absorption peak in the UV region. The high absorption coefficient makes perovskites effective absorber layers in solar cells. Perovskite absorber layers with thickness much smaller than the carrier diffusion length would be favorable for light harvesting, which contributes to a higher open circuit voltage.[21] In Fig. 2(b), the absorption cross-section is deduced by the following formula,

$$\tilde{n} = \frac{mN_A}{M} \qquad N = \frac{\tilde{n}}{V} = \frac{\rho N_A}{M} \qquad \sigma = \frac{\alpha}{N}, \tag{3}$$

where N_A is the Avogadro's number, m is the mass and V is the volume. The density ρ of $CsPbBr_3$ is ca. 4.8 Mg/m^3 refers to SpringerMaterials, the molecular weight M is found to be 579.8 g/mol

and thus the atomic number density N is calculated to be around 5×10^{21} /cm^3. Dividing the absorption coefficient with the N, we can get the absorption cross-section spectrum. The absorption cross-section obtained here can be rescaled for nanocrystals with different sizes[22] and a high absorption cross-section is essential for achieving room temperature continuous wave pumped lasers. In addition, two-photon absorption (TPA) cross-section which is indispensable for nonlinear devices[23] is found to be proportional to the linear absorption cross-section and a reliable linear absorption cross-section is required to reduce the discrepancy of reported values of TPA.[24] The optical conductivity is also computed. It describes the contribution of photogenerated charge carriers to conductivity when the material is under illumination. The conductivity σ equals to the product of the angular frequency ω, the relative imaginary dielectric constant ε_2 in Fig. (1c) and the permittivity in vacuum. The high optical conductivity shown in Fig. 2(c) implies the possible optoelectronic applications such as photodetectors and photovoltaics. Fig. 2(d) shows the dispersion relation ω - k of the exciton resonance. The dispersion relation is obtained by the following formula:

$$Re\{k\} = n(\omega)\omega c^{-1} \text{ and } Im\{k\} = \kappa(\omega)\omega c^{-1}, \quad (4)$$

where ω is the frequency and c is the speed of light in vacuum. The linear fit of the dispersion relation gives a slope of 1.53×10^8 m/s, which is the velocity of light travelling in perovskite material. The circuitous part at the resonance frequency exhibits the typical dispersion relation of a polariton with damping. Although the photons and the excitations are often treated as independent quantities, there exists coupling between the incident electromagnetic field and the generated electromagnetic field by oscillating polarization of an optical excitation, and a polariton is created as a result of the light-matter interplay. It should be noted that the polariton here implies the coupling between excitons and free space photon modes rather than the coupling between

excitons and cavity photon modes. Here we illustrate an exciton associated polariton, where the linear part of the dispersion shows the uncoupled photon propagation and the circuitous part embodies the coupling between the exciton and the visible light, which detours the original linear propagation.

In order to study the change of optical properties and three-dimensional Wannier-Mott exciton behaviors with temperature, temperature dependent reflection spectroscopy was performed. To our knowledge, temperature dependent reflection spectroscopy was never conducted before on $CsPbBr_3$ bulk crystals. The reflection spectroscopy can be used to precisely determine the transition energy positions and directly reveals the joint density of states unlike photoluminescence spectroscopy which involves carrier relaxation process. The reflection spectroscopy on bulk crystal is one of the most comprehensive way to study the electronic system of a material.[25]

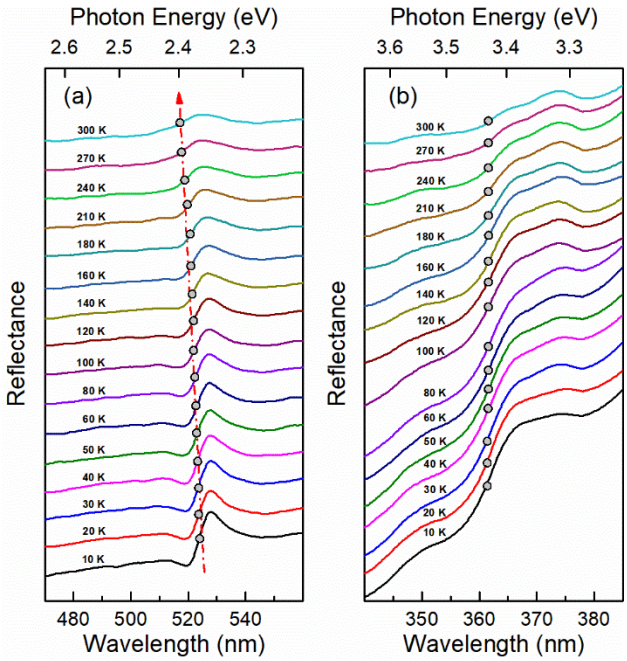

FIG. 3. The temperature dependent reflectance on the $CsPbBr_3$ bulk crystal sample (a) around the excitonic absorption region in the visible range and (b) in the UV range. The grey dots indicate the point of inflection and the red dash arrow serves as a guide to the eye. Spectra are vertically shifted for clarity.

As shown in the temperature dependent reflectance in Fig. 3(a), the excitonic absorption is obvious from 10 K to room temperature. The similar line shapes were reported in other semiconductors with excitons forming at direct bandgaps.[26] The existence of the excitonic peak in room temperature (also from Fig. 1(c), Fig. 2(a)) indicates that the exciton binding energy is at least above the thermal energy k_BT (k_B is the Boltzmann constant and T is the temperature) at room temperature, which is around 26 meV. The blue shift of the exciton absorption peak with temperature is indicated by the inflection point and arrow in Fig. 3(a). This unconventional blue shift is commonly observed in lead based material[27] and caused by the contribution of Pb 6s orbital to the valence band maximum of perovskites by antibonding.[28] We will show detail analysis of temperature dependent excitonic features in Fig. 4. In Fig. 1(b), the temperature dependent

reflection at UV region is shown. While the excitonic peak is blue shifted with temperature, the energy position of the peak at UV region is almost invariant with temperature or even with a very slight red shift. This invariance is due to the joint effect of the thermal expansion of the lattice structure and the phonon-electron scattering.[29] The exciton in the visible range is attributed to the lowest-energy direct transition at R point in the first Brillion zone while the peak at UV region is the second lowest energy transition attributed mainly to the M point, consistent with results from previous first principle study[30] of $CsPbBr_3$ and the optical transitions identified by ellipsometry. The different behaviors of the transitions with respect to temperature at different critical points R and M in the Brillion zone unveil the complexity of the phonon-electron scattering in perovskites. Previous studies on hybrid perovskites also reported peaks with different shifts and attributed the phenomenon to coexisting phases or organic cations,[31] however inorganic perovskite $CsPbBr_3$ have no organic cations nor phase transitions in the measurement range. A more inclusive model for perovskite material family is needed to explain this observation, also taking account of Rashba effect,[32] spin-orbital coupling, crystal field and all other intriguing phenomenon of perovskites.

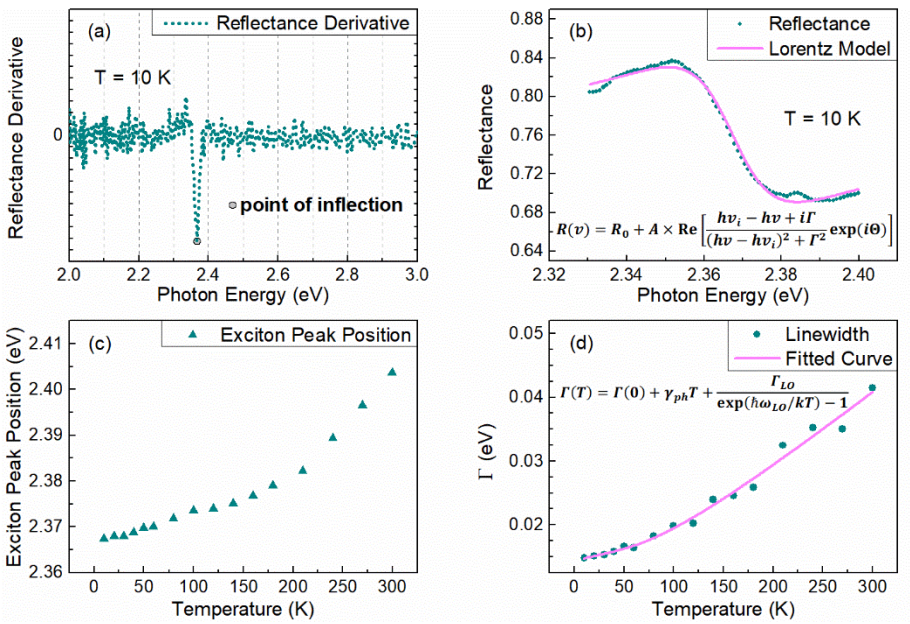

FIG. 4. Exciton peak positions and widths. (a) The point of inflection method to determine the peak position from derivative reflectance spectrum at 10 K. The grey dot indicates the inflection point. (b) The fit of the Lorentzian model to the reflectance spectrum at 10 K. (c) Excitonic peak positions and (d) Γ with respect to temperature. The blue dots are the experiment data and the pink solid line is the fitted curve in (b) and (d).

To extract the peak position and the linewidth of the excition transition, we use a lorentzian dispersion model[11, 33-36] to describe the reflectance line shape:

$$R(v) = R_0 + A \times \mathrm{Re}\left[\frac{hv_i - hv + i\Gamma}{(hv - hv_i)^2 + \Gamma^2}\exp(i\Theta)\right], \quad (5)$$

where R_0 is the background reflection, A is the amplitude, hv_i is the transition energy, Γ is the broadening or damping and Θ is the phase factor. In Fig. 4(b), we show the fitting of the reflectance at 10 K, which gives us a transition energy of 2.367 eV, same with the result using point of inflection method[37-38] by first derivative of the reflectance in Fig. 4(a). This validates the reliabity of the Lorentzian model. Whereas the derivative spectrum gradually becomes noisy when

temperature rises, the Lorentzian model is utilized from 10K to room temperature for consistency. Peak positions and peak widths at different temperatures are summarized in Fig. 4(c) and 4(d). In Fig. 4(d), we apply the formula $\Gamma(T) = \Gamma(0) + \gamma_{ph}T + \Gamma_{LO}/[\exp(\hbar\omega_{LO}/kT) - 1]$,[39-40] where $\Gamma(0)$ is the broadening at 0 K, γ_{ph} is the acoustic phonon coupling strength and $\hbar\omega_{LO}$ is the optical phonon energy. The fitting results gives γ_{ph} around 35.56 μeV/K and that the optical phonon energy around 25 meV, which is close to the results from previous studies.[41-44] The larger contribution of optical phonons compared with acoustic ones to the linewidth broadening is ubiquitous for polar semiconductors, which was also reported in hybrid perovskites.[45] We also observed a slightly decrease of the intensity of the reflection spectrum with temperature, which suggests a slightly decrease of the dielectric constant when temperature increases. The alike phenomenon was also found in hybrid perovskites[46] and other lead composed semiconductors such as PbTe, PbSe and PbS.[47]

Finally, the longitudinal-transverse splitting observed as a stop band in reflectance spectrum can be extrapolated to acquire the oscillator strength. A large oscillator strength is indispensable for prominent optical phenomenon and for applications such as exciton-polariton lasers.[48-49] Employ the formula below

$$\omega_L - \omega_T = \frac{f}{2\omega_T \varepsilon_b}, \tag{6}$$

where ω_T is the transverse resonance frequency equals 3.57×10^{15} rad/sec while ω_L is the longitudinal resonance equals 3.62×10^{15} rad/sec. Both parameters are deduced from the stop band structure in the reflectance spectrum at 10 K.[50] With the assumption that the damping is small at 10 K, the longitudinal-transverse splitting can be approximately estimated by the energy separation

between the maximum and minimum of the reflectance line shape. Here ε_b is the background dielectric constant around the exciton resonance. From Fig. 1(c), we can see that the dielectric constant is different when approaching the excitonic peak from different side of the photon energy. ε_b is around 3.69 at the high energy side, which is slightly lower than the low energy side of the dielectric constant ε_s around 3.73. The calculated oscillator strength is found to be 1.3×10^{30} rad^2/sec^2 (~0.02 per formula unit), comparable with hybrid perovskites.[51] According to the Lyddane–Sachs–Teller (LST) relation,[52]

$$\frac{{\omega_L}^2}{{\omega_T}^2} = \frac{\varepsilon_s}{\varepsilon_b}. \quad (7)$$

We assess that $3.73/3.69$ equals 1.011, and $(\omega_L/\omega_T)^2$ equals 1.028. The accordance of the theory and the experiment result corroborates the reliability of the estimation. The large oscillator strength, high refractive index and facile shape control of perovskite material make it a favorable candidate for an exciton-polariton laser as both a gain material and a cavity itself.

CONCLUSIONS

In summary, $CsPbBr_3$ bulk crystal was investigated by temperature dependent reflection spectroscopy and ellipsometry. We infer the intrinsic exciton properties like the exciton transition energy, the exciton oscillator strength, exciton polariton as well as the exciton-phonon interaction. In addition to critical optical transitions and wavelength dependent optical constants, essential information such as absorption coefficient, absorption cross-section, optical conductivity and dispersion relation are also acquired. This work provides significant information on the

fundamental photophysics of $CsPbBr_3$ and would be helpful for practical applications based on inorganic perovskites.

AUTHOR INFORMATION

Corresponding Author

*E-mail: hdsun@ntu.edu.sg.

ACKNOWLEDGMENTS

This research was supported by the Singapore Ministry of Education through the Academic Research Fund under Projects MOE2016-T2-1-054, Tier 1-RG105/16, Tier 1-RG92/15 and Tier 1-RG189/17 (S). H.Z. wishes to thank the National Science Fund for Distinguished Young Scholars of China (61604074).

REFERENCES

(1) Kovalenko, M. V.; Protesescu, L.; Bodnarchuk, M. I. Properties and Potential Optoelectronic Applications of Lead Halide Perovskite Nanocrystals. *Science* **2017,** *358*, 745-750.

(2) Adinolfi, V.; Peng, W.; Walters, G.; Bakr, O. M.; Sargent, E. H. The Electrical and Optical Properties of Organometal Halide Perovskites Relevant to Optoelectronic Performance. *Adv. Mater.* **2018,** *30*, 1700764.

(3) Wang, Y.; Sun, H. D. All-Inorganic Metal Halide Perovskite Nanostructures: From Photophysics to Light-Emitting Applications. *Small Methods* **2018,** *2*, 1700252.

(4) Wang, Y.; Li, X. M.; Nalla, V.; Zeng, H. B.; Sun, H. D. Solution-Processed Low Threshold Vertical Cavity Surface Emitting Lasers from All-Inorganic Perovskite Nanocrystals. *Adv. Funct. Mater.* **2017,** *27*, 1605088.

(5) Wang, Y.; Li, X. M.; Song, J. Z.; Xiao, L.; Zeng, H. B.; Sun, H. D. All-Inorganic Colloidal Perovskite Quantum Dots: A New Class of Lasing Materials with Favorable Characteristics. *Adv. Mater.* **2015,** *27*, 7101-7108.

(6) Li, W. W.; Sha, T. T.; Wang, Y.; Yu, W. L.; Jiang, K.; Zhou, H.; Liu, C.; Hu, Z. G.; Chu, J. H. Effects of Deposition Methods and Processing Techniques on Band Gap, Interband Electronic Transitions, and Optical Absorption in Perovskite $CH_3NH_3PbI_3$ Films. *Appl. Phys. Lett.* **2017,** *111*, 011906.

(7) Hoshi, K.; Chiba, T.; Sato, J.; Hayashi, Y.; Takahashi, Y.; Ebe, H.; Ohisa, S.; Kido, J. Purification of Perovskite Quantum Dots Using Low-Dielectric-Constant Washing Solvent "Diglyme" for Highly Efficient Light-Emitting Devices. *ACS Appl. Mater. Interfaces* **2018,** *10*, 24607-24612.

(8) Yamanaka, T.; Masumori, K.; Ishikawa, R.; Ueno, K.; Shirai, H. Role of Isopropyl Alcohol Solvent in the Synthesis of Organic-Inorganic Halide $CH(NH_2)_2PbI_xBr_{3-x}$ Perovskite Thin Films by a Two-Step Method. *J. Phys. Chem. C* **2016,** *120*, 25371-25377.

(9) Wang, Y.; Sun, H. D. Advances and Prospects of Lasers Developed from Colloidal Semiconductor Nanostructures. *Prog. Quantum Electron.* **2018,** *60*, 1-29.

(10) Grancini, G.; Kandada, A. R. S.; Frost, J. M.; Barker, A. J.; De Bastiani, M.; Gandini, M.; Marras, S.; Lanzani, G.; Walsh, A.; Petrozza, A. Role of Microstructure in the Electron-Hole Interaction of Hybrid Lead Halide Perovskites. *Nat. Photonics* **2015,** *9*, 695-701.

(11) Tilchin, J.; Dirin, D. N.; Maikov, G. I.; Sashchiuk, A.; Kovalenko, M. V.; Lifshitz, E. Hydrogen-Like Wannier-Mott Excitons in Single Crystal of Methylammonium Lead Bromide Perovskite. *Acs Nano* **2016,** *10*, 6363-6371.

(12) Song, J. Z.; Cui, Q. Z.; Li, J. H.; Xu, J. Y.; Wang, Y.; Xu, L. M.; Xue, J.; Dong, Y. H.; Tian, T.; Sun, H. D.; et al. Ultralarge All-Inorganic Perovskite Bulk Single Crystal for High-Performance Visible-Infrared Dual-Modal Photodetectors. *Adv. Opt. Mater.* **2017,** *5*, 1700157.

(13) *Spectroscopic Ellipsometry for Photovoltaics;* Fujiwara, H., Collins, R. W., Eds.; Springer: Switzerland, 2018.

(14) Sapori, D.; Kepenekian, M.; Pedesseau, L.; Katan, C.; Even, J. Quantum Confinement and Dielectric Profiles of Colloidal Nanoplatelets of Halide Inorganic and Hybrid Organic-Inorganic Perovskites. *Nanoscale* **2016,** *8*, 6369-6378.

(15) Sha, W. E. I.; Ren, X. G.; Chen, L. Z.; Choy, W. C. H. The Efficiency Limit of $CH_3NH_3PbI_3$ Perovskite Solar Cells. *Appl. Phys. Lett.* **2015,** *106*, 221104.

(16) Ball, J. M.; Stranks, S. D.; Hoerantner, M. T.; Huettner, S.; Zhang, W.; Crossland, E. J. W.; Ramirez, I.; Riede, M.; Johnston, M. B.; Friend, R. H.; et al. Optical Properties and Limiting Photocurrent of Thin-Film Perovskite Solar Cells. *Energy Environ. Sci.* **2015,** *8*, 602-609.

(17) Werner, J.; Niesen, B.; Ballif, C. Perovskite/Silicon Tandem Solar Cells: Marriage of Convenience or True Love Story? - An Overview. *Adv. Mater. Interfaces* **2018,** *5*, 1700731.

(18) Chen, C. W.; Hsiao, S. Y.; Chen, C. Y.; Kang, H. W.; Huang, Z. Y.; Lin, H. W. Optical Properties of Organometal Halide Perovskite Thin Films and General Device Structure Design Rules for Perovskite Single and Tandem Solar Cells. *J. Mater. Chem. A* **2015,** *3*, 9152-9159.

(19) Loper, P.; Stuckelberger, M.; Niesen, B.; Werner, J.; Filipic, M.; Moon, S. J.; Yum, J. H.; Topic, M.; De Wolf, S.; Ballif, C. Complex Refractive Index Spectra of $CH_3NH_3PbI_3$ Perovskite Thin Films Determined by Spectroscopic Ellipsometry and Spectrophotometry. *J. Phys. Chem. Lett.* **2015,** *6*, 66-71.

(20) Green, M. A.; Ho-Baillie, A.; Snaith, H. J. The Emergence of Perovskite Solar Cells. *Nat. Photonics* **2014,** *8*, 506-514.

(21) Huang, J.; Yuan, Y.; Shao, Y.; Yan, Y. Understanding the Physical Properties of Hybrid Perovskites for Photovoltaic Applications. *Nat. Rev. Mater.* **2017,** *2*, 17042.

(22) Xia, C. H.; Wu, W. W.; Yu, T.; Xie, X. B.; van Oversteeg, C.; Gerritsen, H. C.; Donega, C. D. Size-Dependent Band-Gap and Molar Absorption Coefficients of Colloidal $CuInS_2$ Quantum Dots. *Acs Nano* **2018,** *12*, 8350-8361.

(23) Wang, Y.; Li, X. M.; Zhao, X.; Xiao, L.; Zeng, H. B.; Sun, H. D. Nonlinear Absorption and Low-Threshold Multiphoton Pumped Stimulated Emission from All-Inorganic Perovskite Nanocrystals. *Nano Lett.* **2016,** *16*, 448-453.

(24) Chen, J. S.; Zidek, K.; Chabera, P.; Liu, D. Z.; Cheng, P. F.; Nuuttila, L.; Al-Marri, M. J.; Lehtivuori, H.; Messing, M. E.; Han, K. L.; et al. Size- and Wavelength-Dependent Two-Photon Absorption Cross-Section of $CsPbBr_3$ Perovskite Quantum Dots. *J. Phys. Chem. Lett.* **2017,** *8*, 2316-2321.

(25) Kittel, C. *Introduction to Solid State Physics*; Wiley: New York, 2004.

(26) Sell, D. D.; Dingle, R.; Stokowski, S. E.; DiLorenzo, J. V. Observation of Polaritons in GaAs: A New Interpretation of the Free-Exciton Reflectance and Luminescence. *Phys. Rev. Lett.* **1971,** *27*, 1644-1647.

(27) Dey, P.; Paul, J.; Bylsma, J.; Karaiskaj, D.; Luther, J. M.; Beard, M. C.; Romero, A. H. Origin of the Temperature Dependence of the Band Gap of PbS and PbSe Quantum Dots. *Solid State Commun.* **2013,** *165*, 49-54.

(28) Frost, J. M.; Butler, K. T.; Brivio, F.; Hendon, C. H.; van Schilfgaarde, M.; Walsh, A. Atomistic Origins of High-Performance in Hybrid Halide Perovskite Solar Cells. *Nano Lett.* **2014,** *14*, 2584-2590.

(29) Varshni, Y. P. Temperature Dependence of Energy Gap in Semiconductors. *Physica* **1967,** *34*, 149-154.

(30) Protesescu, L.; Yakunin, S.; Bodnarchuk, M. I.; Krieg, F.; Caputo, R.; Hendon, C. H.; Yang, R. X.; Walsh, A.; Kovalenko, M. V. Nanocrystals of Cesium Lead Halide Perovskites ($CsPbX_3$, X = Cl, Br, and I): Novel Optoelectronic Materials Showing Bright Emission with Wide Color Gamut. *Nano Lett.* **2015,** *15*, 3692-3696.

(31) Huang, W.; Yue, S. Z.; Liu, Y.; Zhu, L. P.; Jin, P.; Wu, Q.; Zhang, Y.; Chen, Y. A.; Liu, K.; Liang, P.; et al. Observation of Unusual Optical Band Structure of $CH_3NH_3PbI_3$ Perovskite Single Crystal. *Acs Photonics* **2018,** *5*, 1583-1590.

(32) Isarov, M.; Tan, L. Z.; Bodnarchuk, M. I.; Kovalenko, M. V.; Rappe, A. M.; Lifshitz, E. Rashba Effect in a Single Colloidal $CsPbBr_3$ Perovskite Nanocrystal Detected by Magneto-Optical Measurements. *Nano Lett.* **2017,** *17*, 5020-5026.

(33) Boyd, R. W. *Nonlinear Optics*; Elsevier: San Diego, 2008.

(34) Korona, K. P.; Wysmolek, A.; Pakula, K.; Stepniewski, R.; Baranowski, J. M.; Grzegory, I.; Lucznik, B.; Wroblewski, M.; Porowski, S. Exciton Region Reflectance of Homoepitaxial GaN Layers. *Appl. Phys. Lett.* **1996,** *69*, 788-790.

(35) Jiang, H.; Zhao, G. Y.; Ishikawa, H.; Egawa, T.; Jimbo, T.; Umeno, M. Determination of Exciton Transition Energy and Bowing Parameter of AlGaN Alloys in AlGaN/GaN Heterostructure by Means of Reflectance Measurement. *J. Appl. Phys.* **2001,** *89*, 1046-1052.

(36) Yang, Z.; Surrente, A.; Galkowski, K.; Bruyant, N.; Maude, D. K.; Haghighirad, A. A.; Snaith, H. J.; Plochocka, P.; Nicholas, R. J. Unraveling the Exciton Binding Energy and the Dielectric Constant in Single-Crystal Methylammonium Lead Triiodide Perovskite. *J. Phys. Chem. Lett.* **2017,** *8*, 1851-1855.

(37) Raja, A.; Chaves, A.; Yu, J.; Arefe, G.; Hill, H. M.; Rigosi, A. F.; Berkelbach, T. C.; Nagler, P.; Schuller, C.; Korn, T.; et al. Coulomb Engineering of the Bandgap and Excitons in Two-Dimensional Materials. *Nat. Commun.* **2017,** *8*, 15251.

(38) Chernikov, A.; Berkelbach, T. C.; Hill, H. M.; Rigosi, A.; Li, Y. L.; Aslan, O. B.; Reichman, D. R.; Hybertsen, M. S.; Heinz, T. F. Exciton Binding Energy and Nonhydrogenic Rydberg Series in Monolayer WS_2. *Phys. Rev. Lett.* **2014,** *113*, 076802.

(39) Oneill, M.; Oestreich, M.; Ruhle, W. W.; Ashenford, D. E. Exciton Radiative Decay and Homogeneous Broadening in CdTe/$Cd_{0.85}Mn_{0.15}$Te Multiple-Quantum Wells. *Phys. Rev. B* **1993,** *48*, 8980-8985.

(40) Makino, T.; Chia, C. H.; Tuan, N. T.; Segawa, Y.; Kawasaki, M.; Ohtomo, A.; Tamura, K.; Koinuma, H. Exciton Spectra of ZnO Epitaxial Layers on Lattice-Matched Substrates Grown with Laser-Molecular-Beam Epitaxy. *Appl. Phys. Lett.* **2000,** *76*, 3549-3551.

(41) Ramade, J.; Andriambariarijaona, L. M.; Steinmetz, V.; Goubet, N.; Legrand, L.; Barisien, T.; Bernardot, F.; Testelin, C.; Lhuillier, E.; Bramati, A.; et al. Exciton-Phonon Coupling in a $CsPbBr_3$ Single Nanocrystal. *Appl. Phys. Lett.* **2018,** *112*, 072104.

(42) Sebastian, M.; Peters, J. A.; Stoumpos, C. C.; Im, J.; Kostina, S. S.; Liu, Z.; Kanatzidis, M. G.; Freeman, A. J.; Wessels, B. W. Excitonic Emissions and above-Band-Gap Luminescence in the Single-Crystal Perovskite Semiconductors $CsPbBr_3$ and $CsPbCl_3$. *Phys. Rev. B* **2015,** *92*, 235210.

(43) Stoumpos, C. C.; Malliakas, C. D.; Peters, J. A.; Liu, Z. F.; Sebastian, M.; Im, J.; Chasapis, T. C.; Wibowo, A. C.; Chung, D. Y.; Freeman, A. J.; et al. Crystal Growth of the Perovskite Semiconductor $CsPbBr_3$: A New Material for High-Energy Radiation Detection. *Cryst. Growth Des.* **2013,** *13*, 2722-2727.

(44) Iaru, C. M.; Geuchies, J. J.; Koenraad, P. M.; Vanmaekelbergh, D.; Silov, A. Y. Strong Carrier - Phonon Coupling in Lead Halide Perovskite Nanocrystals. *Acs Nano* **2017,** *11*, 11024-11030.

(45) Wright, A. D.; Verdi, C.; Milot, R. L.; Eperon, G. E.; Perez-Osorio, M. A.; Snaith, H. J.; Giustino, F.; Johnston, M. B.; Herz, L. M. Electron-Phonon Coupling in Hybrid Lead Halide Perovskites. *Nat. Commun.* **2016,** *7*, 11755.

(46) Jiang, Y. J.; Soufiani, A. M.; Gentle, A.; Huang, F. Z.; Ho-Baillie, A.; Green, M. A. Temperature Dependent Optical Properties of $CH_3NH_3PbI_3$ Perovskite by Spectroscopic Ellipsometry. *Appl. Phys. Lett.* **2016,** *108*, 061905.

(47) Zemel, J. N.; Jensen, J. D.; Schoolar, R. B. Electrical and Optical Properties of Epitaxial Films of PbS, PbSe, PbTe, and SnTe. *Phys. Rev.* **1965,** *140*, A330-A342.

(48) Faist, J.; Capasso, F.; Sirtori, C.; Sivco, D. L.; Hutchinson, A. L.; Cho, A. Y. Laser Action by Tuning the Oscillator Strength. *Nature* **1997,** *387*, 777-782.

(49) Fraser, M. D.; Hofling, S.; Yamamoto, Y. Physics and Applications of Exciton-Polariton Lasers. *Nat. Mater.* **2016,** *15*, 1049-1052.

(50) Klingshirn, C. F. *Semiconductor Optics*; Springer: Germany, 2012.

(51) Ishihara, T. Optical Properties of PbI-Based Perovskite Structures. *J. Lumin.* **1994,** *60-1*, 269-274.

(52) Fox, M. *Optical Properties of Solids*; Oxford University Press: New York, 2010.

TOC Graphic

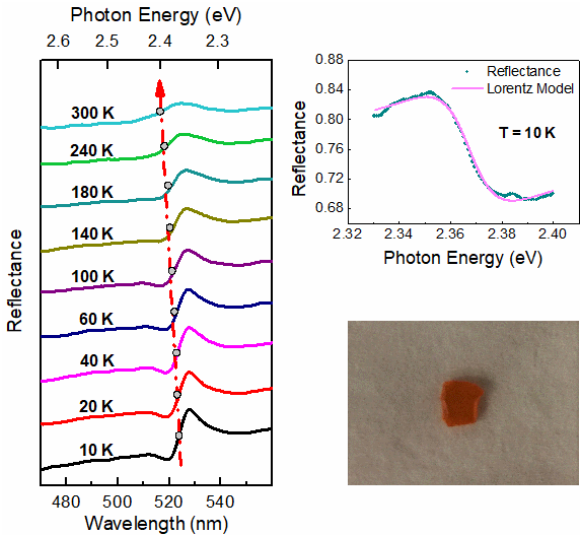
Photon Energy (eV)
2.6
2.5
2.4
2.3
300 K
240 K
180 K
140 K
100 K
60 K
40 K
20 K
10 K
Reflectance
480
500
520
540
Wavelength (nm)
Reflectance
Lorentz Model
T = 10 K
0.88
0.84
0.80
0.76
0.72
0.68
Reflectance
2.32
2.34
2.36
2.38
2.40
Photon Energy (eV)